A fluorescent reporter enables instantaneous measurement of cell cycle speed in live cells

Anna E. Eastman[1,2], Xinyue Chen[1,2], Xiao Hu[1,2], Amaleah A. Hartman[1,2], Aria M. Pearlman Morales[3], Cindy Yang[4], Jun Lu[2,5], Hao Yuan Kueh[6], and Shangqin Guo[1,2]

[1]Department of Cell Biology, Yale University, New Haven, CT, USA; [2]Yale Stem Cell Center, Yale University, New Haven, CT, USA; [3]Department of Biomedical Engineering, Yale University, New Haven, CT, USA; [4]Department of Molecular, Cellular, and Developmental Biology, Yale University, New Haven, CT, USA; [5]Department of Genetics. Yale University, New Haven, CT, USA; [6]Department of Bioengineering, University of Washington, Seattle, WA, USA

Correspondence should be addressed to Shangqin Guo. Email: shangqin.guo@yale.edu
Address: 10 Amistad St. Room 131H, New Haven, CT 06520
Phone: 203-737-6411, fax: 203-785-4305

Abstract

Periodicity is a fundamental property of biological oscillators such as the mitotic cell cycle. In this context, periodicity refers to the time interval between the same phases of two consecutive cell cycles. The length of this interval, or the cell cycle speed, varies widely depending on cell type and the pathophysiological conditions. The relevance of cell cycle speed in various biological contexts has not been well-studied, partially due to the lack of experimental approaches that capture this parameter. Here, we describe a genetically encoded live-cell reporter of cell cycle speed. This reporter is based on the color-changing Fluorescent Timer (FT) protein, which emits blue fluorescence when newly synthesized before maturing into a red fluorescent protein. Its ability to report cell cycle speed exploits the different half-life of the blue vs. red form of the same molecule, as predicted by mathematical modeling. When a Histone H2B-FT fusion protein is expressed at steady-state in heterogeneously dividing cells, faster-cycling cells can be distinguished from slower-cycling ones by differences in their intracellular ratio between the blue and red fluorescent wavelengths. Cell cycle perturbation experiments demonstrate that the H2B-FT is a *bona fide* reporter of cell cycle speed in multiple cultured cell lines. *In vivo*, the blue/red profile faithfully tracked with known proliferation kinetics of various hematopoietic stem and progenitor cells, when expressed either from lentiviral vectors or from a targeted knock-in allele. As the H2B-FT is compatible with flow cytometry, it provides a strategy to physically separate subpopulations of live cells cycling at different rates for downstream analysis. We anticipate this system to be useful in diverse cell types and tissue contexts for dissecting the role of cell cycle speed in development and disease.

Main

Cell cycle speed varies widely during development and tissue homeostasis, linking characteristic cycling behavior with unique aspects of biology[1,2]. Across most of the animal kingdom, the cleavage divisions initiating embryonic development follow well-defined rapid and synchronous mitotic cycles[3]. Cell cycles lengthen and become heterogeneous at the onset of gastrulation[4,5]. In mammals, a characteristically fast cell cycle is seen in embryonic stem cells (ESCs) derived from the inner cell mass[6]. Transition out of pluripotency, both *in vitro* and *in vivo*, is coupled with dramatic restructuring and lengthening of the cell cycle[6,7]. Post-development, highly regulated cell cycles are seen across many tissue types including blood[8,9], brain[10], intestine[11], and others[12,13]. In adult mice, it is estimated that most hematopoietic stem cells (HSCs) divide rarely [14], and the ability to maintain quiescence is essential for their function[8]. Contrastingly, committed myeloid progenitors proliferate rapidly under homeostasis[15]. Granulocyte-macrophage progenitors (GMPs) in particular appear to be one of the most proliferative cell types[15], and are known to possess unique cell fate plasticity beyond the hematopoietic fate[16,17]. Besides illustrating the natural diversity in cell cycle behaviors, these cell types provide valuable systems to gauge the validity of novel tools for cell cycle studies.

Abnormal cell cycle is characteristic of certain disease states such as cancer. Many oncogenes and tumor suppressor genes, such as Rb, p53 and c-Myc[18-20], converge on the (dys)regulation of the cell cycle. Conventional chemotherapies often attempt to blunt cancer growth by targeting the cell cycle[21,22], but the efficacy could be compromised by natural heterogeneity in the proliferative behavior of the cancer cells[23]. Relapse due to development of chemo-resistance is thought to be related to the presence of quiescent cancer cells at the time of treatment[24]. Cell cycle control is equally important in non-malignant cell proliferation, especially for homeostatic control in tissues of rapid turnover, such as the skin and intestinal epithelium[25,26]. In tissues where cellular turnover is low, for example the heart, the inability of cells to re-enter the cell cycle appears to underlie the tissue's poor regenerative capacity[27]. Overall, understanding the consequences of diverse cycling behaviors in development, regeneration, and disease is of fundamental importance. However, convenient assessment of cell cycle speed, especially in live cells *in vivo*, remains technically challenging.

Currently available strategies for cell cycle analysis have several limitations. First, they mostly focus on specific cell cycle phases[28-30], but not speed. While a fast-dividing cell population usually contains a greater proportion of S/G2/M cells at any given time, any single cell could be transiting through these phases irrespective of its cell cycle speed. Second, although image tracking of consecutive mitoses is direct and accurate for determining cell cycle length, many cells *in vivo* are not amenable to direct imaging. Additionally, at least two mitoses need to occur for microscopy-based cell cycle quantification.

Further, microscopy-based identification does not enable physical separation of fast- vs. slow-cycling cells for downstream molecular or functional assays. Third, while various label retention techniques have yielded much of our current knowledge on stem cell quiescence *in vivo*[12,14,31], the cycling kinetics of dividing cells become difficult to resolve after they lose their label during the chase period. Label retention assays, either in the form of generic dyes[32], nucleotide analogs, or genetically encoded H2B-GFP, reflect the cell divisional history during the chase period, but give little information about the current cycling state. The resolution of such methods is also limited by how similar the cells are to each other[16]. Some of the labels are also cytotoxic, or require fixation to visualize[14]. To overcome the above-mentioned limitations, we implemented a genetically encoded color-changing fluorescent protein which reports on cell cycle speed in a ratiometric manner. This reporter is suitable for cell cycle studies of live cells both *in vitro* and *in vivo*.

Results

Mathematical modeling predicts that molecules of unequal half-lives are differentially susceptible to molecular halving by cell division

The steady state level of a given molecule is determined by the sum of its biogenesis and turnover. Molecular turnover occurs by active catalysis or by passive dilution when cells divide. The extent to which cell division contributes to molecular turnover depends on a given molecule's half-life (Equation S1). When the time scale of turnover is significantly shorter than the length of the cell cycle, the contribution from active turnover dominates. An example of this is the inhibitor of NF-κB, or IκBa, which undergoes enhanced degradation upon phosphorylation within minutes of signaling, leading to NF-κB activation[33]. However, when turnover is slow and approaches the length of the cell cycle, reduction in the number of molecules by cell division becomes the main mode of their removal. This phenomenon is seen in PU.1 accumulation during myeloid fate commitment[34]. The different behaviors of short- vs. long-lived molecules in relation to the cell cycle length are illustrated in Fig. 1a. The intracellular concentration of a stable molecule varies more than that of an unstable molecule in response to cell division rate, suggesting a potential strategy for ranking cells according to their cell cycle length by expressing two molecules, e.g. fluorescent proteins, of unequal half-lives.

To exploit the differential susceptibility of labile and stable molecular species to cell division-mediated halving, we turned our attention to the Fluorescent Timer (FT)[35]. The FT is a color-changing protein that emits blue fluorescence when newly synthesized, and irreversibly turns red after a characteristic time delay[35] (Fig. 1b, Extended Data Fig. S1a). The blue and red proteins are synthesized

orthogonally in a stoichiometric 1:1 manner, because the blue species is a folding intermediate of the red, whose abundance can be measured separately by fluorescence microscopy and/or by flow cytometry. Importantly, the immature blue form of the FT is lost quickly after synthesis when it changes into the red form, which has a much longer half-life (Fig. 1b, Extended Data Fig. S1a). Thus, the blue form represents the short-lived molecule, whose concentration is less variable across the cell cycle as compared to the stable red form (Extended Data Fig. S1b-d). From a mathematical model describing the kinetics of fluorescence conversion and subsequent degradation, we find that the steady-state blue/red fluorescence ratio scales inversely with cell cycle length (Equation S2), with a shorter (longer) cell cycle length giving rise to a higher (lower) blue/red ratio. Thus, the blue/red FT ratio decreases as the cell cycle lengthens or slows (Fig. 1c, Extended Data Fig. S1b-d), providing a potential strategy to distinguish live cells of different cycling rates (Fig. 1d).

H2B-FT fusion proteins undergo blue to red conversion, and the red fluorescence is stable

To render the FT useful for microscopy-based quantitation, the FT was fused to the C-terminus of histone H2B (Fig. 2a). This localized the FT signal to the chromatin (Fig. 2b), facilitating nuclear segmentation and image processing. To assess whether tagging the FT onto a histone interferes with its color-changing properties, we imaged Hela cells expressing the H2B-FT under the control of a Tetracycline-inducible (TetO) promoter (Fig. 2a). HeLa cells transduced with the "Medium" FT variant[35] (Extended Data Fig. S1a) began to produce detectible blue signal ~2 hours after adding doxycycline (Dox) to the culture medium (Fig. 2c-d, Extended Data Movie 1), a time delay presumably required for Dox-induced transcription and translation. Approximately 1.5 hours after the first appearance of blue fluorescence, red signal emerged as the first wave of FT molecules underwent maturation (Fig. 2c, Extended Data Movie 1). The average level of red fluorescence per nucleus continued to increase over the next 26 hours until reaching steady-state fluorescence (Fig. 2e), i.e. the level of fluorescence in cells continuously maintained in Dox. By contrast, the average level of blue fluorescence plateaued much sooner (after ~7 hours) (Fig. 2d), as expected for a molecule which is lost (in this case converted to red) shortly after synthesis. To confirm the divergent turnover times for the blue and red FT, we treated cells with Dox briefly ("Dox Pulse", Fig. 2f). Upon Dox washout, blue signal dropped below detectible levels within 7 hours, while red signal persisted for the remainder of the imaging experiment, >24 hours (Fig. 2e-f), confirming that the red H2B-FT is more stable than the blue form.

To further assess the stability of H2B-FT-red and gain insights into the contribution by potential cell division-independent reduction in the red fluorescence, we tracked single cells (primary mouse embryonic

fibroblasts (MEFs) or Hela) over time after Dox washout (Extended Data Fig. S2a-b). In MEFs, the red fluorescence decreased slowly in the absence of mitosis, while mitosis led to a ~50% drop in red fluorescence (Extended Data Fig. S2a,c). The underlying reason for slow or no division did not matter, as irradiated MEFs and non-dividing MEFs naturally existing in active cultures behaved identically (Extended Data Fig S2c). Alternatively, we tracked the combined red fluorescence intensity from all progeny arising from single Hela cells by mitosis (Extended Data Fig. S2b,d). Similar to MEFs, mitosis caused ~50% drop in red fluorescence, as long as all the progeny were accounted for (Extended Data Fig. S2d). Of note, the half-life we obtained for the red species in the absence of mitosis was ~84 hours in MEFs and ~37 hours in Hela, in both cases substantially longer than the 24-hour half-life reported for the FT[35]. The increased H2B-FT stability could result from being fused to a core histone, which are among the most stable proteins[36]. These results also suggest that the resolution of the H2B-FT as a cell cycle speed reporter could become limited in the extremely slowly dividing cells, where non-division mediated decay could no longer be ignored.

Mathematical simulation of the FT behavior predicts that it reports cell cycle speed only after its expression reaches steady-state (Extended Data Fig. S1b-d). When expression is first induced, the blue form should be over-represented independently of cell cycle effects because insufficient time has elapsed for the red molecules to accumulate. In agreement with the model, cells displayed higher blue/red ratio within the first 24 hours of Dox induction as compared to cells maintained continuously in Dox (Fig. 2g, Extended Data Movies 1 and 2). As such, all subsequent experiments described below were conducted after the cells had been exposed to Dox for sufficient time (≥2 days) to reach steady-state H2B-FT expression.

H2B-FT blue/red ratio responds to cell cycle manipulation in cultured cells

As discussed above, the mathematical model predicts that cell cycle acceleration would cause the blue/red ratio to increase, while cell cycle lengthening would lead to the opposite effect. To test this experimentally, we perturbed the cell cycle by several different methods in cultured cells expressing the H2B-FT.

We first accelerated cell proliferation by c-Myc expression in primary MEFs carrying allelic expression of the H2B-FT[37] (details below), specifically the FT-Medium variant (Extended Data Fig. S1a). Following overnight transduction with c-Myc or an empty vector (EV) control virus, the H2B-FT fluorescence was determined by quantitative time-lapse microscopy (Extended Data Fig. S3). As expected, cells overexpressing c-Myc proliferated more rapidly (Fig. 3a). On the population level, c-Myc-

transduced MEFs displayed a higher blue/red ratio than control MEFs after 70 hours but not at 25 hours post-transduction (Fig. 3b), which was presumably before the exogenously expressed c-Myc had significantly altered the cell cycle. Notably, the blue/red ratio was heterogeneous at the single-cell level in both control and c-Myc-expressing cultures (Fig. 3c). To determine whether this heterogeneity reflected cell cycle speed heterogeneity, we categorized cells based on their relative blue/red ratio following a FACS-style gating strategy (Fig. 3c), and systematically determined individual cell cycle lengths by tracking the time interval between two consecutive mitoses within the same cell lineage. In c-Myc transduced cultures, there were more cells in the high blue/red ratio group ("Blue cells") and fewer cells of low blue/red ratio ("Red cells") (Fig. 3c-d). Importantly, the blue cells divided faster than the red cells in both conditions (Fig. 3e). While most red cells had a long cell cycle (>30 hours), the blue cell cycle length centered around 10-15 hours/cycle in the control culture and 5-10 hours/cycle in the c-Myc-transduced culture (Fig. 3e, blue cells). A small population (~1.5%) of c-Myc transduced cells had a cell cycle length shorter than 5 hours/cycle (Fig. 3e). Interestingly, for most of the cells that had an intermediate level of blue/red ratio (cells between the gates in Fig. 3c), their cell cycle length appeared to center around 25 hours/cycle, likely representing the gap between the fast dividing blue cells and the slow dividing red cells (Fig. 3e). These results are in good agreement with previous reports of MEF proliferation[6]. Importantly, the blue/red ratio of individual cells reflected cell cycle rates regardless of whether they had been transduced with c-Myc. In either case, cells with the highest blue/red ratio divided faster (Fig. 3e-f). As such, the blue/red ratio of H2B-FT reports cell proliferation rate at both the population and single-cell level.

To test whether cell cycle lengthening would decrease the blue/red ratio, we expressed the H2B-FT in BaF3 cells, whose rapid proliferation is dependent on IL-3[38]. To slow their proliferation, BaF3 cells initially cultured in high IL-3 (270ng/mL) were switched to lower IL-3 levels (14ng/µl). Within 48 hours after switching, BaF3 cells cultured in low IL-3 displayed reduced proliferation, which completely ceased in IL-3 free conditions (Fig. 4a). The blue/red fluorescence intensity of BaF3 cells cultured in these conditions were measured by flow cytometry. This analysis revealed that BaF3 cells grown in high IL-3 largely emitted blue fluorescence, which shifted toward the red axis at low IL-3 and became entirely red with IL-3 withdrawal (Fig. 4b).

Since the absolute level of intracellular H2B-FT protein varies, it is challenging to directly compare the raw blue/red ratio across different cells. To overcome this limitation, we instead use the normalized blue/red ratio, which is given by dividing the blue signal intensity with the total combined blue and red signal intensity per cell:

$$\text{Normalized } \frac{\bar{B}}{\bar{R}} = \frac{\bar{B}}{\bar{B}+\bar{R}}$$

This places all cells on a scale of 0-1, 0 being all red and 1 being all blue (Fig. 4c). All graphs involving blue/red ratio were normalized in this manner. As expected, the blue/red ratio of BaF3 cells decreased in response to cell cycle lengthening (Fig. 4c). IL-3-induced differences in proliferation were captured by all three kinetic variants of the FT protein: H2B-FT-Fast, H2B-FT-Medium, and H2B-FT-Slow (Extended Data Fig. S4). Furthermore, as predicted by Equation S2, the range of blue/red ratio was lowest with FT-Fast and highest with FT-Slow (Extended Data Fig. S4), which have the shortest and longest blue-to-red conversion time, respectively (Extended Data Fig. S1a). For simplicity, all data presented from here on were obtained with the FT-Medium.

To examine the response of H2B-FT in a situation where cell cycle speed changes due to complex regulations such as differentiation, we assessed mouse embryonic stem cells (mESCs) with allelic expression of H2B-FT[37] (details below and Fig. 4d). mESCs have a characteristic cell cycle of 8-10 hours that immediately lengthens upon differentiation[6]. Taking advantage of this natural change in cell cycle rate, we induced mESC differentiation with retinoic acid (RA)[39] (Extended Data Fig. S5), which slowed the cell cycle as confirmed by EdU/DAPI staining (Fig. 4e). As expected, mESCs treated with RA for 48 hours displayed a profound, population-wide shift toward the red-axis (Fig. 4f). Only incomplete differentiation was expected, since the RA treatment was brief. This partial differentiation strategy yielded cell state heterogeneity, which was captured by the prominently red-shifted, but overlapping, population following RA treatment (Fig. 4f). Taken together, our results demonstrate that the H2B-FT blue/red ratio responds to diverse modes of cell cycle manipulations in multiple cell types.

H2B-FT blue/red profile enables FACS sorting of live cells with different cycling rates

We wished to test the feasibility of using the blue/red profile to physically separate live cell populations with distinct proliferation dynamics. To do this, mESCs kept in pluripotency maintenance conditions or treated with RA as described above were assessed in more detail. We separated the cells based on their blue/red intensities (Fig. 4g-h) and compared their cell cycle profile by DNA content staining (Fig. 4i). As cells with longer cell cycles tend to increase their dwell time in G1 phase relative to other phases, we expect slow-dividing cells to be enriched for G1 cells. Consistently, the reddest population (Fig. 4g-j, Red) was enriched for G1 phase cells, while the bluest (Fig. 4g-j, Blue) contained a larger proportion of G2/M cells. Cells from the middle FT gate (Fig. 4g-j, Middle) had an intermediate cell cycle profile. This was not only the case for the RA-treated samples, but also for cells that had been

kept in pluripotency maintenance conditions (Fig. 4g-j). These findings further validate that the H2B-FT blue/red ratio reports proliferation rate, and agree with observations that pluripotent stem cells do not respond homogeneously or synchronously to differentiation induction[40,41].

To evaluate functional heterogeneity associated with the H2B-FT color profile, cells from individual blue/red gates were FACS-sorted and re-plated in pluripotency conditions to evaluate their ability to give rise to new alkaline phosphatase (AP)-expressing colonies[42]. We expected the slow-cycling (red) cells to be more differentiated and have reduced ability to form colonies, and that any cells which had not exited pluripotency during the RA treatment to be among the fastest-cycling (blue) group. In concordance with the DAPI/EdU results, RA treatment greatly reduced the overall colony-forming activity (Fig. 4k). Importantly, the residual colony-forming potential was most enriched in the blue cells and depleted in the red ones (Fig. 4k, right). Our results also demonstrated that even among cells never induced to differentiate, colony forming potential was highest within the bluest cells, albeit this difference was less pronounced (Fig. 4k, left), corroborating reports that cellular heterogeneity exists under pluripotency maintenance conditions[43,44] and is often associated with the cell cycle[43,45]. These results confirmed the presence of cell cycle heterogeneity in both culture conditions which could be captured and sorted by FACS using the H2B-FT reporter.

The proliferative landscape of live hematopoietic cells as captured by the H2B-FT

To test whether the H2B-FT can report cell cycle speed *in vivo*, we took advantage of the well-known proliferative differences[15] in hematopoietic stem and progenitor cells (HSPCs). For a first approach, the H2B-FT was virally introduced into donor HSCs, which were subsequently transplanted into recipient mice. Following engraftment and reconstitution, we analyzed the hematopoietic stem cells and multipotent progenitors (Lin-Kit+Sca+, LKS), the granulocyte-macrophage progenitors (GMPs) and the whole bone marrow (WBM) (Extended Data Fig. S6a-b, gating strategy). The heterogeneity as reflected by the blue/red profile was most exaggerated in the WBM (Fig. 5a-b), consistent with the fact that WBM contains the entire dynamic spectrum from rapidly-cycling progenitors to post-mitotic differentiated cells. By contrast, the GMPs and LKS cells displayed narrower distributions (Fig. 5a-b). Among the HSPCs positive for H2B-FT, LKS cells were red-shifted as compared to the GMPs (Fig. 5a-b). This was expected because the LKS compartment contains the more primitive quiescent and slow-cycling hematopoietic progenitors, while the GMPs are highly proliferative[14,15]. These reconstituted LKS cells were heterogeneous, with a subset of them having increased blue signal (Fig. 5a-b), possibly reflecting the more proliferative multipotent progenitors[14,15]. Although the GMPs were collectively bluer than LKS and

many other cells, they were not the bluest within the bone marrow (Fig. 5b). Further investigation revealed the bluest cells to be Ter119+ (Fig. 5c-d), indicating a committed erythroid identity. Contrastingly, Mac1+ myeloid cells displayed a wide blue/red distribution, with a substantial subpopulation severely red-shifted (Fig. 5c-d). These data are consistent with the known proliferative behavior of myeloid and erythroid cells as determined by BrdU uptake kinetics in separate studies[15,46]. Thus, H2B-FT expressed from a lentiviral vector captures heterogeneity associated with distinct proliferative behaviors *in vivo*.

To make the H2B-FT applicable to other cellular systems less amenable to viral transduction, we targeted the H2B-FT coding sequence into the mouse *HPRT* locus[37], under the control of a Dox inducible promoter (Fig. 6a). When crossed with cell type specific rtTA or tTA, H2B-FT expression should be induced in desired cell types. To test the utility of this mouse model, we crossed the H2B-FT KI allele with the Rosa26:rtTA[47], which enabled inducible H2B-FT (iH2B-FT) expression in most tissues including the hematopoietic system. The compound mice were healthy and fertile (data not shown). To directly compare the proliferative behavior of erythroid progenitors and GMPs in the same animal, we injected mice with EdU and analyzed the cell cycle profile of CD71+/Ter119+ cells and GMPs 2 hours later (Extended Data Fig. S6a-c, gating strategy). Approximately 40% of the erythroid cells, as compared to 27% of GMPs, incorporated EdU within the labeling period (Fig. 6b), confirming that the CD71+/Ter119+ cells were indeed more proliferative than GMPs. Accordingly, the CD71+/Ter119+ cells were further blue-shifted as compared to GMPs (Fig. 6c), similar to the results obtained with the viral approach (Fig. 5). When the HSPCs from Dox-treated animals were analyzed, the LKS compartment was again robustly red-shifted and heterogeneous (Fig. 6c), also in agreement with the virally expressed H2B-FT (Fig. 5a-b). Thus, the cycling rates of primary bone marrow cells are faithfully reflected by the H2B-FT blue/red ratio.

Circulating blood cells primarily consist of B cells (B220+), T cells (CD3+) and neutrophils/monocytes (Mac1+) (Fig. 6d), with the myeloid cells turning over more rapidly than the lymphocytes in normal hematopoiesis[15]. To test whether this difference is reflected by the H2B-FT, we analyzed the blue/red profile of the peripheral blood mononuclear cells (PBMN) from iH2B-FT mice maintained on Dox. For unclear reasons, fewer cells expressed detectible H2B-FT in blood (~30%, Fig. 6e, top) as compared to bone marrow (>95%, data not shown). Importantly however, of the H2B-FT+ cells in blood, Mac1+ cells were bluer than B220+ or CD3+ cells, whose blue/red profiles were highly heterogeneous (Fig. 6e, top). The B and T compartments contained a severely red-shifted subpopulation which could represent long-lived memory cells[48]. Although the exact identity and function of these

various cellular subsets remain to be determined, FACS based separation should provide a convenient approach for their further study.

Lastly, we explored the iH2B-FT blue/red profile in a disease state characterized by overt proliferation, such as acute myeloid leukemia (AML). To induce AML, we crossed the iH2B-FT allele with a Dox inducible MLL-ENL (iMLL-ENL) allele targeted into the *Col1a* locus[49]. Mice harboring both the iH2B-FT and iMLL-ENL were treated with Dox. As expected, the myeloid compartment expanded within 2 weeks, when the bone marrow contained a preponderance of L-GMPs (Extended Data Fig. S6d) and the blood became dominated by Mac1+ cells (Fig. 6d-e, Extended Data Fig. S6e, bottom). The expanded myeloid compartment was immediately visible by the increased number of H2B-FT+ cells in the unstained whole blood (Fig. 6e, bottom). Further, the bluest-shifted subpopulation was ~3x larger than that in healthy control mice. Overall, the distinct proliferative behaviors of normal, as well as malignant, hematopoietic cells can be readily detected by FACS based on their H2B-FT blue/red ratio.

H2B-FT blue/red ratio provides an estimate of cell cycle length *in vivo*

Since the H2B-FT blue/red ratio qualitatively agreed with known proliferative behaviors across various biological settings, we sought to determine cell cycle lengths in a more quantitative manner. The mathematical model (Equation S2) describes a relationship between the steady-state blue/red ratio, $\frac{\bar{B}}{\bar{R}}$, and the cell cycle length, τ_D:

$$\frac{\bar{B}}{\bar{R}} = \frac{C \cdot \tau_C}{\tau_D}$$

This equation suggests that the cell cycle length τ_D varies as a function of $\frac{\bar{B}}{\bar{R}}$ and could be derived if the constant *C* can be experimentally determined, as the color conversion time τ_C remains the same for a given FT variant (Extended Data Fig. S1a). With the normalized $\frac{\bar{B}}{\bar{R}}$ value as discussed above, the modified Equation S2b becomes

$$\frac{\bar{B}}{\bar{B} + \bar{R}} = \frac{C \cdot \tau_C}{C \cdot \tau_C + \tau_D}$$

We found that *C* depended on the fluorescence detection parameters: exposure time in the case of fluorescence microscopy, and laser voltage for flow cytometry (Extended Data Fig. S7). To determine the value of *C*, we measured the cell cycle lengths for iH2B-FT GMPs during a 24-hour culture period by live cell imaging and single cell tracking (Fig. 7a). After 24 hours, the imaged iH2B-FT GMPs were analyzed

by FACS to determine their blue/red profile (Fig. 7b). With the assumption that the blue/red ratio is directly related to cell cycle speed (as supported by Fig. 3), these experiments provided the values for $\frac{\bar{B}}{\bar{B}+\bar{R}}$ and cell cycle length τ_D such that the value of a combined constant $C \cdot \tau_C$ could be determined (Fig. 7a-d). Similar results were obtained based on the estimates from the 10th, 25th, 50th and 80th percentile of cell cycle length, assumed to correspond to the 90th, 75th, 50th and 20th percentile of the bluest cells, respectively (Fig. 7c-d). As MEFs and HeLa cells displayed H2B-FT-red decay independent of cell division (Extended Data Fig. S2), we considered a modified version of Equation S2 in which a rate constant for active degradation, τ_R, was incorporated into the red removal rate, δ:

$$\delta = \frac{1}{\tau_R} + \frac{1}{\tau_D}$$

However, this modified equation yielded values that fitted poorly with the cell cycle lengths of cultured GMPs as determined by image tracking; the shorter the input red half-life, the worse the fit. The best fit came from ignoring τ_R ($\frac{1}{\tau_R} \to 0$), when δ becomes simply inversely proportional to τ_D. We therefore proceeded to estimate cell cycle length assuming little contribution from cell division-independent decay.

Having determined the value of $C \cdot \tau_C$, we went on to estimate the cell cycle lengths for various hematopoietic cell types. Specifically, we assessed the H2B-FT blue/red ratio in mature monocytes and granulocytes[50] as well as immunophenotypically defined stages of erythropoiesis[51] (Extended Data Fig. S6f-g, gating strategy). Overall, granulocytes (Gran) were estimated to have an average cell cycle length of >30 hours/cycle. The erythroid progenitors (ProE) appeared to have the shortest cell cycle, averaging at ~4.3 hours/cycle (Fig. 7e). This result was particularly compelling, since it agrees nicely with fetal liver ProE cell cycle length previously determined using sequential thymidine labeling[52]. L-GMPs from iMLL-ENL mice had a wider range of cell cycle speeds than normal GMPs, but the median shifted toward a shortened cell cycle length of ~9 hours/cycle (Fig. 7f). For most examined populations, the cell cycle length distributions were similar from animal to animal, and the variability generally decreased as the population became more immunophenotypically defined (Fig. 7g). High variability was seen in whole bone marrow, which was expected for a heterogeneous tissue. However, one cell type broke this pattern: among LKS cells, we observed variability comparable to that of the whole bone marrow (Fig. 7g). The range and center of the LKS cycling speed distribution varied substantially across individual mice, while GMPs were more uniform with an estimated median cell cycle length of ~11.6 hours/cycle (Fig. 7g-h). The variability among LKS cells revealed by H2B-FT implies novel biology to be further studied. Taken together, the H2B-FT blue/red profile could help to estimate the *in vivo* cell cycle lengths.

Discussion

An inherent aspect of cell cycle is the component of time, which is usually difficult to determine from measurements made at static time points. Taking advantage of the distinct life spans of a single molecule when it exists in two fluorescently distinct states, we have established a novel method for determining cell cycle rate of live cells, *in vitro* as well as *in vivo*. The ratio between the two fluorescence intensities, as determined by live cell imaging or flow cytometry, faithfully reflected the proliferative state of all cell types tested. Unlike assays based on label dilution[12,14,31,32], the readout is not restricted to a specific time window because fluorescence from the genetically encoded H2B-FT does not decay over cellular generations. Superior to methods that require cell fixation[14], the fluorescence profile enables physical separation of live cell subpopulations. With this reporter targeted into the mouse genome, even rare cell populations, such as the HSCs, can be reliably analyzed. We have also demonstrated that the H2B-FT can be conveniently expressed, e.g. by a lentiviral vector, to enable the assessment of cell cycle rate in other cellular models, including human cells. Overall, the method described here offers a unique opportunity to assess a fundamental aspect of biology: the speed of the cell cycle, in various biological and disease settings that were previously inaccessible. This represents a first step in capturing the full distribution and modulation of cell cycle lengths *in vivo* in live cells. Given that blue/red ratio changes through the duration of a single cell cycle (Extended Data Fig. S1), we anticipate that resolution could be further improved, for example by effectively synchronizing cells from their most recent mitosis with the help of a cell cycle phase reporter.

The particular proliferative behaviors marking specific cell states are often considered passive in nature. Our previous work witnessed the surprising and extraordinary cell fate plasticity possessed by the naturally fast-dividing GMPs (at ~8 hours per cell cycle) toward pluripotency[16]. The molecular basis underlying this plasticity remains unclear, and represents only one of the numerous cell fate changes coinciding with distinct cell cycle behaviors[1,53]. We anticipate the H2B-FT will be helpful in elucidating the mechanistic basis of cell fate control. Beyond probing basic biology, the method described here should also be applicable to addressing questions of clinical importance. For example, chemotherapy resistance is believed to be mediated by the quiescent subset of cancer cells[24]. Is this indeed the case? If so, does the quiescent subset represent pre-existing intra-tumoral heterogeneity, or they are induced by specific treatment regimens? Further, when expressed specifically in the host, the H2B-FT could also be used to reveal potential proliferation heterogeneity in the complex tumor niche. These questions, among many others, can now be modeled in the H2B-FT mouse.

Beyond its technical utility, the mathematical principles underlying the H2B-FT reporter have important biological implications. The experimental H2B-FT data depict a generalized relationship

between molecular half-life and intracellular concentration. These findings constitute direct evidence for a mechanism by which cells can selectively alter their molecular contents by modulating cell cycle dynamics. Simplistically, intracellular molecules can be placed in two categories: those that exist long enough such that their intracellular concentration is dependent on cell cycle length; and shorter-lived molecules which are less sensitive to dilution by cell division. Since these principles do not discriminate against any specific types of molecule, they suggest a fundamental mechanism by which cell cycle speed might be tuned to optimize the concentration of key molecular regulators, including proteins, their various post-translationally modified derivatives, RNA species, and others. This aspect of regulation could echo the direct regulation on the half-life of proteins and RNAs, since the effective concentration is determined not only by the turnover rate, but also by the cell cycle length.

Methods

Cloning and reporter cell line generation

pFast-FT-N1, pMedium-FT-N1, and pSlow-FT-N1 were obtained from Addgene (31910, 31911, and 31912 respectively). Each FT coding sequence (~711 bp each) was cloned into a Dox-inducible lentiviral backbone and a constitutive retroviral backbone. The inducible lentiviral plasmid (pFU-TetO-Gateway-PGK-Puro) was constructed previously[54] by inserting a Gateway cassette (Thermo Fisher Scientific/Invitrogen), a PGK promoter, and a puromycin resistance gene into the pFU-tetO-Klf4 vector[55] through blunted EcoRI sites. Each FT insert was then cloned into this destination vector through Gateway recombination. For constitutive expression, the FT sequences were inserted into a pSCMV[54] retroviral backbone using HindIII and XhoI restriction sites. The H2B-FT fusion transgenes were constructed by overlap extension PCR using the three FT plasmids as well as the human H2B.J coding sequence from PGK-H2B-mCherry (Addgene # 21217) as templates, and cloned into the pFU-TetO-Gateway-PGK-Puro and pSCMV expression plasmids. H2B-mCherry and H2B-BFP (BFP template from Addgene #52115) inserts were similarly cloned to serve as single-color controls for the color-changing H2B-FT.

The MSCV-IRES-GFP (“empty vector”) retroviral expression plasmid was previously described[56]. The LZRS-c-Myc-IRES-GFP retroviral expression plasmid was a gift from Sebastian Nijman.

Viral vectors were transfected in 293T cells using Fugene® 6 transfection reagent (Promega). Viruses harvested from the supernatant were used to transduce BaF3 and HeLa cells. Successfully transduced cells were selected by FACS.

*HPRT::*iH2B-FT knock-in mouse embryonic stem cells (mESCs) were generated using inducible cassette exchange (ICE) to target the TetO-CMV-H2B-FT transgene to the *HPRT* locus by cre-recombination in the A2lox.cre mESC cell line[37]. Briefly, H2B-FT inserts (all three kinetic variants, Subach et al. and Extended Data Fig. S1a), as well as H2B-BFP and H2B-mCherry were cloned into P2lox targeting plasmids[37] using HindIII and NotI restriction sites. The targeting plasmids were electroporated into Dox-activated A2lox.cre mESCs. After one day of recovery on neomycin-resistant feeder MEFs (Millipore Sigma), successfully recombined clones were selected by supplementing the mESC culture medium with 300µg/mL geneticin (G418). After 6 days of selection, healthy surviving colonies were hand-picked under an inverted microscope and replated onto WT irradiated feeder MEFs. These "Passage 0" cultures were subsequently split for cryopreservation as well as continued culture and characterization of reporter activity by fluorescence microscopy and flow cytometry.

Primer sequences used for cloning are provided in Supplementary Table 1. Plasmid maps are available upon request.

Cell culture and mESC differentiation

MEFs, HeLa, and 293T cells were cultured in a standard growth medium ("MEF medium") consisting of DMEM basal medium (Gibco) with 10% heat-inactivated fetal bovine serum (FBS) (Gibco) and 1% penicillin/streptomycin/L-Glutamine supplement (ThermoFisher). For MEF derivation from E13.5 embryos, this medium was additionally supplemented with 1% Non-essential amino acid (NEAA) mixture (ThermoFisher) for the first passage *in vitro*. 293T cells used for viral transfection were cultured in the standard growth medium additionally supplemented with 1% sodium pyruvate (ThermoFisher). Occasionally, phenol-red-free Medium 199 was used in place of DMEM for live fluorescence microscopy experiments with H2B-FT HeLa cells (details in main text). Mouse embryonic stem cells (mESCs) were cultured either on irradiated feeder MEFs or on plates coated with 0.1% gelatin in DMEM supplemented with 15% ESC-qualified FBS (Millipore), 1% penicillin/streptomycin/L-Glutamine, 1% NEAA, 1000U/ml LIF (Millipore), and 0.8µl/100mL β-mercaptoethanol. BaF3 cells were cultured in an RPMI-based growth medium consisting of 10% heat-inactivated FBS, 1% penicillin/streptomycin/L-Glutamine, and 270pg/mL IL-3 (Peprotech). Primary GMPs were cultured in complete X-vivo medium (Lonza) supplemented with 10% BSA (Stemcell Technologies), 1% penicillin/streptomycin/L-Glutamine, 0.14µl/mL β-mercaptoethanol, and 100 ng/ml mSCF, 50 ng/ml mIL3, 50 ng/ml Flt3L, and 50 ng/ml mTPO (all from PeproTech).

In vitro, doxycycline (Sigma) was added to cell culture medium at 2µg/mL for inducible promoter activation. To induce iH2B-FT and/or iMLL-ENL expression *in vivo*, mice were fed drinking water containing 1g/L Dox supplemented with 10g/L sucrose.

For the differentiation assay, mESCs maintained on Feeder MEFs were transferred to feeder-free conditions (0.1% gelatin) for 2 passages to potentiate exit from pluripotency. The pluripotency of control cells was maintained with mESC culture medium, while the differentiation condition entailed switching the cells into standard MEF medium supplemented with 2µM retinoic acid (RA) (Sigma).

For the colony recovery assay, sorted cells were plated onto feeder MEFs (n = 4 replicate wells) at a standardized seeding density and fed with mESC medium. After 6 days, the cultures were fixed and alkaline phosphatase (AP) staining was done using the Stemgent APII kit in accordance with the protocol provided by the manufacturer. Colonies staining positive for AP activity were counted manually (RA treated group) or using an automated image processing workflow (mESCs).

Total mRNA was extracted with TRIzol® Reagent (Ambion) and reverse transcribed into cDNA using SuperScriptIII™ First-Strand Synthesis SuperMix (Invitrogen) according to the product manual. For quantitative real-time PCR, cDNA and gene-specific primers were mixed with iQ™ SYBR®Green Supermix (Bio-Rad) and carried out using a Bio-Rad CFX384™ Real-Time PCR System. Gene expression levels were normalized to GAPDH level in the same sample. qPCR primer sequences are provided in Supplementary Table 1.

Mice

All mouse work was approved by the Institutional Animal Care and Use Committee (IACUC) of Yale University. All research animals were housed and maintained in facilities of Yale Animal Resource Center (YARC).

HPRT::iH2B-FT-Medium and *HPRT*::iH2B-FT-Slow chimeric mice were generated from passage 0 A2lox.cre H2B-FT targeted mouse embryonic stem cells by the Yale Genome Editing Center via blastocyst injection and implantation into C57/Bl6 females. High-degree chimeric male offspring were selected by coat color and the iH2B-FT allele was subsequently backcrossed onto a C57/Bl6 background. For all H2B-FT blue/red analysis of primary-harvested cells, H2B-FT expression was induced *in vivo* for at least one week by feeding Dox drinking water.

WT feeder MEFs for pluripotent stem cell culture were derived from C57/Bl6 (Jackson Lab) E13.5 mouse embryos and mitotically inactivated by 80 Gy γ-irradiation. H2B-FT-Medium MEFs were derived from *HPRT*::iH2B-FT-Medium E13.5 mouse embryos.

HSPC transplantation

FACS-purified bone-marrow-derived LKS cells from donor mice were transduced overnight *in vitro* with TetO-H2B-FT lentivirus and injected through the tail vein at >10,000 cells/mouse into 9-week-old γ-irradiated recipient mice (9 Gy) along with 500,000 WBM support cells. Alternatively, donor mice were injected intraperitoneally with 150µg/g body weight 5-fluorouracil (5-FU) 4 days before harvesting, and the HSPC-enriched WBM was virally transduced and then transplanted at a ratio of 1 donor per 2 recipients. Transplanted mice were given a one-time intraperitoneal injection of 200µg Dox and thereafter continuously maintained on Dox drinking water. After four weeks, peripheral blood was collected and analyzed by flow cytometry to evaluate H2B-FT expression coming from the engrafted virally transduced cells. Bone marrow HSPCs were harvested between 12-16 weeks post-transplantation and stained with fluorescent antibodies marking Lineage, Kit, Sca-1, CD34, and CD16/32. Cellular fluorescence was recorded on a BD™ LSRII flow cytometer, and the data were subsequently analyzed using FlowJo software (FlowJo, LLC).

A complete list of antibodies used in this study is provided in Supplementary Table 2.

EdU/DAPI labeling

Cultured cells were treated with growth medium containing 10µM EdU for 15 minutes. EdU was rinsed away with PBS and cells were trypsinized into a single-cell suspension for immediate fixation or H2B-FT blue/red FACS-sorting followed by fixation. For *in vivo* labeling, mice were pulsed with EdU at 50µg/g body weight via intraperitoneal injection 2 hours before harvesting. Bone-marrow-derived HSPCs plus Ter119+ cells were enriched via streptavidin-conjugated magnetic microbead separation (Miltenyi Biotec, Product #130-048-101) of lineage+ cells (lineage cocktail included biotin-conjugated CD3e, CD4, CD8, CD11b, Gr1, and B220), stained with GMP markers or CD71/Ter119, and sorted by FACS on a BD™ FACSAria directly into 70% ethanol. These fixed single-cell suspensions of EdU-treated cells were stored in 70% ethanol at -20C for >24h, and then rinsed in PBS. Cells were permeablized in 0.2% Triton X-100 in PBS at room temperature for 15 minutes and then fluorescently labeled by Click chemistry using a Click-IT EdU-488 kit (ThermoFisher Scientific, Product #C10337) for 30 minutes at room temperature in an AF488-azide EdU labeling cocktail prepared according to the product manual. Cells were rinsed in PBS and incubated for 10 minutes at room temperature in 1µg/mL DAPI (ThermoFisher Scientific #D1306) diluted in PBS. Cells were rinsed once more with PBS and resuspended in a PBS buffer containing 1% BSA, then analyzed by flow cytometry on a BD LSRII.

Microscopy

Live-cell microscopy was performed using a Molecular Devices ImageXpress® Micro 4 high-throughput compound inverted epifluorescence microscope equipped with a live imaging environment. For time lapse imaging, cells were plated into a Greiner Bio-One CellStar® 96well plate, sealed with a Breathe-Easy® gas-permeable membrane, and maintained at 37C/5% CO2 for the duration of the experiment. MetaXpress® 6 software was used for all image acquisition and for some image processing and analysis. Most of the image segmentation and image-based measurements were carried out using CellProfiler™ and exported into FCS Express 6 Image Cytometry software (De Novo™ Software) for data analysis. CellProfiler™ pipelines and sample raw images from our experiments are available on request.

Statistical Information

Details pertaining to each statistical analysis are provided in the figure legend accompanying the relevant data figure. All statistical tests used were two-tailed.

Data Availability Statement

The data that support the findings of this study are available from the corresponding author upon reasonable request.

References

1 Chen, X., Hartman, A. & Guo, S. Choosing Cell Fate Through a Dynamic Cell Cycle. *Current Stem Cell Reports* **1**, 129-138, doi:10.1007/s40778-015-0018-0 (2015).

2 Soufi, A. & Dalton, S. Cycling through developmental decisions: how cell cycle dynamics control pluripotency, differentiation and reprogramming. *Development* **143**, 4301-4311, doi:10.1242/dev.142075 (2016).

3 O'Farrell, P. H., Stumpff, J. & Su, T. T. Embryonic Cleavage Cycles: How Is a Mouse Like a Fly? *Curr Biol* **14**, R35-45 (2004).

4 Newport, J. & Kirschner, M. A major developmental transition in early Xenopus embryos: I. characterization and timing of cellular changes at the midblastula stage. *Cell* **30**, 675-686 (1982).

5 Deneke, V. E., Melbinger, A., Vergassola, M. & Di Talia, S. Waves of Cdk1 activity in S-phase synchronize the cell cycle in Drosophila embryos. *Dev Cell* **38**, 399-412 (2016).

6 White, J., Dalton, S. Cell Cycle Control of Embryonic Stem Cells. *Stem Cell Reviews* **1**, 8 (2005).

7 Calder, A. *et al.* Lengthened G1 phase indicates differentiation status in human embryonic stem cells. *Stem Cells Dev* **22**, 279-295, doi:10.1089/scd.2012.0168 (2013).

8 Pietras, E. M., Warr, M. R. & Passegue, E. Cell cycle regulation in hematopoietic stem cells. *J Cell Biol* **195**, 709-720, doi:10.1083/jcb.201102131 (2011).

9 Orford, K. W. & Scadden, D. T. Deconstructing stem cell self-renewal: genetic insights into cell-cycle regulation. *Nat Rev Genet* **9**, 115-128, doi:10.1038/nrg2269 (2008).

10 Yoshikawa, K. Cell cycle regulators in neural stem cells and postmitotic neurons. *Neurosci Res* **37**, 1-14 (2000).
11 van der Flier, L. G. & Clevers, H. Stem cells, self-renewal, and differentiation in the intestinal epithelium. *Annu Rev Physiol* **71**, 241-260, doi:10.1146/annurev.physiol.010908.163145 (2009).
12 Tumbar, T. *et al.* Defining the Epithelial Stem Cell Niche in Skin. *Science* **303**, 359-363 (2004).
13 Liu, S., Dontu, G. & Wicha, M. S. Mammary stem cells, self-renewal pathways, and carcinogenesis. *Breast Cancer Research* **7**, 86, doi:10.1186/bcr1021 (2005).
14 Wilson, A. *et al.* Hematopoietic stem cells reversibly switch from dormancy to self-renewal during homeostasis and repair. *Cell* **135**, 1118-1129, doi:10.1016/j.cell.2008.10.048 (2008).
15 Passegue, E., Wagers, A. J., Giuriato, S., Anderson, W. C. & Weissman, I. L. Global analysis of proliferation and cell cycle gene expression in the regulation of hematopoietic stem and progenitor cell fates. *J Exp Med* **202**, 1599-1611, doi:10.1084/jem.20050967 (2005).
16 Guo, S. *et al.* Nonstochastic reprogramming from a privileged somatic cell state. *Cell* **156**, 649-662, doi:10.1016/j.cell.2014.01.020 (2014).
17 Ye, M. *et al.* Hematopoietic differentiation is required for initiation of acute myeloid leukemia. *Cell Stem Cell* **17**, 611-623 (2015).
18 Knudsen, E. S. & Wang, J. Y. Targeting the RB-pathway in cancer therapy. *Clin Cancer Res* **16**, 1094-1099, doi:10.1158/1078-0432.ccr-09-0787 (2010).
19 Chen, J. The Cell-Cycle Arrest and Apoptotic Functions of p53 in Tumor Initiation and Progression. *Cold Spring Harb Perspect Med* **6**, a026104, doi:10.1101/cshperspect.a026104 (2016).
20 Gabay, M., Li, Y. & Felsher, D. W. MYC activation is a hallmark of cancer initiation and maintenance. *Cold Spring Harb Perspect Med* **4**, doi:10.1101/cshperspect.a014241 (2014).
21 Schwartz, G. K. & Shah, M. A. Targeting the cell cycle: a new approach to cancer therapy. *J Clin Oncol* **23**, 9408-9421, doi:10.1200/jco.2005.01.5594 (2005).
22 Hamilton, E. & Infante, J. R. Targeting CDK4/6 in patients with cancer. *Cancer Treat Rev* **45**, 129-138, doi:10.1016/j.ctrv.2016.03.002 (2016).
23 Fisher, R., Pusztai, L. & Swanton, C. Cancer heterogeneity: implications for targeted therapeutics. *Br J Cancer* **108**, 479-485, doi:10.1038/bjc.2012.581 (2013).
24 Chen, W., Dong, J., Haiech, J., Kilhoffer, M. C. & Zeniou, M. Cancer Stem Cell Quiescence and Plasticity as Major Challenges in Cancer Therapy. *Stem Cells Int* **2016**, 1740936, doi:10.1155/2016/1740936 (2016).
25 Greco, V. & Guo, S. Compartmentalized organization: a common and required feature of stem cell niches? *Development* **137**, 1586-1594, doi:10.1242/dev.041103 (2010).
26 Li, L. & Clevers, H. Coexistence of quiescent and active adult stem cells in mammals. *Science* **327**, 542-545, doi:10.1126/science.1180794 (2010).
27 Tzahor, E. & Poss, K. D. Cardiac regeneration strategies: Staying young at heart. *Science* **356**, 1035-1039, doi:10.1126/science.aam5894 (2017).
28 Hagting, A., Jackman, M., Simpson, K. & Pines, J. Translocation of cyclin B1 to the nucleus at prophase requires a phosphorylation-dependent nuclear import signal. *Curr Biol* **9**, 680-689 (1999).
29 Sakaue-Sawano, A. *et al.* Visualizing spatiotemporal dynamics of multicellular cell-cycle progression. *Cell* **132**, 487-498, doi:10.1016/j.cell.2007.12.033 (2008).
30 Bajar, B. T. *et al.* Fluorescent indicators for simultaneous reporting of all four cell cycle phases. *Nat Methods* **13**, 993-996, doi:10.1038/nmeth.4045 (2016).
31 Falkowska-Hansen, B. *et al.* An inducible Tet-Off-H2B-GFP lentiviral reporter vector for detection and in vivo isolation of label-retaining cells. *Exp Cell Res* **316**, 1885-1895, doi:10.1016/j.yexcr.2010.02.015 (2010).

32 Lyons, A. B., Hasbold, J. & Hodgkin, P. D. Flow cytometric analysis of cell division history using dilution of carboxyfluorescein diacetate succinimidyl ester, a stably integrated fluorescent probe. *Methods Cell Biol* **63**, 375-398 (2001).

33 Hacker, H. & Karin, M. Regulation and function of IKK and IKK-related kinases. *Sci STKE* **2006**, re13, doi:10.1126/stke.3572006re13 (2006).

34 Kueh, H. Y., Champhekar, A., Nutt, S. L., Elowitz, M. B. & Rothenberg, E. V. Positive feedback between PU.1 and the cell cycle controls myeloid differentiation. *Science* **341**, 670-673, doi:10.1126/science.1240831 (2013).

35 Subach, F. V. *et al.* Monomeric fluorescent timers that change color from blue to red report on cellular trafficking. *Nat Chem Biol* **5**, 118-126, doi:10.1038/nchembio.138 (2009).

36 Toyama, B. H. *et al.* Identification of long-lived proteins reveals exceptional stability of essential cellular structures. *Cell* **154**, 971-982, doi:10.1016/j.cell.2013.07.037 (2013).

37 Iacovino, M. *et al.* Inducible cassette exchange: a rapid and efficient system enabling conditional gene expression in embryonic stem and primary cells. *Stem Cells* **29**, 1580-1588 (2011).

38 Ajjappala, B. S. *et al.* 14-3-3 gamma is stimulated by IL-3 and promotes cell proliferation. *J Immunol* **182**, 1050-1060 (2009).

39 Wichterle, H., Lieberam, I., Porter, J. A. & Jessell, T. M. Directed differentiation of embryonic stem cells into motor neurons. *Cell* **110**, 385-397 (2002).

40 Drukker, M. *et al.* Isolation of primitive endoderm, mesoderm, vascular endothelial and trophoblast progenitors from human pluripotent stem cells. *Nat Biotechnol* **30**, 531-542, doi:10.1038/nbt.2239 (2012).

41 Semrau, S. *et al.* Dynamics of lineage commitment revealed by single-cell transcriptomics of differentiating embryonic stem cells. *Nat Commun* **8**, 1096, doi:10.1038/s41467-017-01076-4 (2017).

42 Sela, Y., Molotski, N., Golan, S., Itskovitz-Eldor, J. & Soen, Y. Human embryonic stem cells exhibit increased propensity to differentiate during the G1 phase prior to phosphorylation of retinoblastoma protein. *Stem Cells* **30**, 1097-1108, doi:10.1002/stem.1078 (2012).

43 Furusawa, T. *et al.* Gene expression profiling of mouse embryonic stem cell subpopulations. *Biol Reprod* **75**, 555-561, doi:10.1095/biolreprod.105.049502 (2006).

44 Stewart, M. H. *et al.* Clonal isolation of hESCs reveals heterogeneity within the pluripotent stem cell compartment. *Nat Methods* **3**, 807-815, doi:10.1038/nmeth939 (2006).

45 Gonzales, K. A. *et al.* Deterministic Restriction on Pluripotent State Dissolution by Cell-Cycle Pathways. *Cell* **162**, 564-579, doi:10.1016/j.cell.2015.07.001 (2015).

46 Pop, R. *et al.* A Key Commitment Step in Erythropoiesis Is Synchronized with the Cell Cycle Clock through Mutual Inhibition between PU.1 and S-Phase Progression. *PLoS Biol* **8** (2010).

47 Hochedlinger, K., Yamada, Y., Beard, C. & Jaenisch, R. Ectopic expression of Oct-4 blocks progenitor-cell differentiation and causes dysplasia in epithelial tissues. *Cell* **121**, 465-477, doi:10.1016/j.cell.2005.02.018 (2005).

48 Tough, D. F. & Sprent, J. Life span of naive and memory T cells. *Stem Cells* **13**, 242-249, doi:10.1002/stem.5530130305 (1995).

49 Ugale, A. *et al.* Hematopoietic stem cells are intrinsically protected against MLL-ENL-mediated transformation. *Cell Rep* **9**, 1246-1255, doi:10.1016/j.celrep.2014.10.036 (2014).

50 Lagasse, E. & Weissman, I. L. Flow cytometric identification of murine neutrophils and monocytes. *J Immunol Methods* **197**, 139-150 (1996).

51 Koulnis, M. *et al.* Identification and Analysis of Mouse Erythroid Progenitors using the CD71/TER119 Flow-cytometric Assay. *J Vis Exp* (2011).

52 Hwang, Y. *et al.* Global increase in replication fork speed during a p57(KIP2)-regulated erythroid cell fate switch. *Sci Adv* **3**, e1700298, doi:10.1126/sciadv.1700298 (2017).

53 Boward, B., Wu, T. & Dalton, S. Concise Review: Control of Cell Fate Through Cell Cycle and Pluripotency Networks. *Stem Cells* **34**, 1427-1436, doi:10.1002/stem.2345 (2016).

54 Guo, S. *et al.* Complex oncogene dependence in microRNA-125a-induced myeloproliferative neoplasms. *Proc Natl Acad Sci U S A* **109**, 16636-16641, doi:10.1073/pnas.1213196109 (2012).

55 Stadtfeld, M., Maherali, N., Breault, D. T. & Hochedlinger, K. Defining molecular cornerstones during fibroblast to iPS cell reprogramming in mouse. *Cell Stem Cell* **2**, 230-240, doi:10.1016/j.stem.2008.02.001 (2008).

56 Lu, J. *et al.* MicroRNA-mediated control of cell fate in megakaryocyte-erythrocyte progenitors. *Dev Cell* **14**, 843-853, doi:10.1016/j.devcel.2008.03.012 (2008).

Acknowledgements

This work was funded by a National Institutes of Health award (DP2GM123507-01); the Charles H. Hood Foundation; and Gilead Sciences. A.E.E. was supported in part by the NIH/NIGMS Cellular and Molecular Biology Training Program under award number T32GM007223. The authors would like to thank the Yale Stem Cell Center, the Yale Cooperative Center for Excellence in Hematology, Dr. Diane Krause (for providing feedback and reagents), the Yale Flow Cytometry Core, and the Yale Genome Editing Core.

Author Contributions

A.E.E. and S.G. conceived and designed experiments. A.E.E., X.C., X.H., A.M.P.M., and S.G. performed experiments. A.E.E., A.M.P.M., and C.Y. analyzed data. X.C., X.H., A.A.H., and J.L. provided samples. H.Y.K. wrote the mathematical equations. A.M.P.M. and J.L. assisted with mathematical modeling. X.C., X.H., A.A.H., J.L., and H.Y.K. assisted A.E.E. and S.G. with critical feedback and data interpretation. A.E.E. and S.G. prepared figures and wrote the manuscript.

Figure Legends

Fig. 1. Design principles of a fluorescent reporter of cell cycle speed. a. Based on Equation S1, intracellular levels of a given molecule, *M*, are predicted to depend on its molecular half-life as well as the cell cycle length. Here, the ratio of *M*'s concentration in theoretical cell populations with different cycling speeds are plotted. When *M* is short-lived (circle, far left), its cellular concentration shows little difference between slow- and fast-cycling cells. However, with a long-lived *M* (circle, far right), the concentration difference increases proportionally to the difference in cell cycle lengths. **b.** The color-changing Fluorescent Timer ("FT") displays a short half-life as a blue protein, and a long half-life as a red protein. **c.** The average blue/red ratio of cells expressing the FT is predicted to drop as cell cycle lengthens (see Equation S2), providing a fluorescence-based strategy to identify cells cycling at different rates. Because the blue/red ratio fluctuates when cell cycle progresses (see Extended Data Fig. S1), the relationship between blue/red ratio and cell cycle length is best described by a probability distribution. For modeling, all cells are assumed to maintain a constant cycling rate through generations. Solid and dashed error bars denote 1 and 2 standard deviations, respectively. All FT blue/red ratio are defined as blue / (blue + red).

d. The anticipated positions of slow and fast cycling cells on a hypothetical plot of blue and red fluorescence intensity.

Fig. 2. Characterization of the H2B-FT reporter in cultured cells. a. Schematic of inducible H2B-FT expression construct. **b.** Representative images of HeLa cells expressing the H2B-FT. **c.** Selected time series of H2B-FT fluorescence in HeLa cells from a representative field of view following doxycycline (Dox) induction. **d-e**. Quantification of average nuclear blue (**d**) and red (**e**) FT intensity over time following Dox treatment. **f.** Selected time series of HeLa cells after Dox washout at T=4.5 h. **g**. Data from (d-e) plotted as blue/red ratio. Error bars represent standard deviation across n = 3 culture wells. Nuclear intensity measurements were normalized to timepoint 0. Images were taken using a 20x objective. Scale bars: 50μm.

Fig. 3. The H2B-FT blue/red profile reflects cell proliferation rate *in vitro*. a. Changes in cell number over time in primary iH2B-FT MEFs following transduction with either c-Myc or empty vector control (EV). Error bars denote standard deviation across n=4 culture wells. **b.** The ratio of blue/red fluorescence intensity was determined for individual cells at 25h and 70h post transduction. Box plots represent the median and interquartile range and whiskers represent 5th-95th percentile. P values were calculated from Mann-Whitney test with a 99% confidence level. 25h, p= 0.295; 70h, p< 0.0001. **c.** The blue and red fluorescence level of individual cells at 70h post transduction. Each dot denotes a single cell. FACS-style gates were applied to representative scatter plots. **d.** The percentage of cells within each gate. Error bars show standard deviation across n=4 culture wells. P=0.0018 (Red Cells) and P=0.0220 (Blue Cells), determined using the Holm-Sidak test. **e.** The cell cycle lengths of individual cells from each gate were determined by image tracking. Cell cycle length represents the time interval between two consecutive mitoses within the same cell lineage. Cell cycle length is heterogeneous and the distribution of cell cycle lengths for each condition are shown as histograms. n values refer to the number of cells tracked for each condition. **f.** The relationship between cell cycle length and H2B-FT blue/red ratio. Each dot denotes an individual cell. All trackable cells (n=189) from both conditions are plotted. Spearman correlation coefficient = -0.7808. P<0.0001 was calculated with a 95% confidence interval.

Fig. 4. H2B-FT blue/red profile allows FACS sorting of live cells with different proliferative rates. a. BaF3 cells proliferate at different rates in varying IL-3 concentrations, as determined by cell counting. Error bars denote standard deviation across n=6 culture wells. **b.** Representative FACS plots of BaF3 cells expressing the H2B-FT reporter grown under different IL-3 concentrations. **c.** Histograms of blue/red fluorescence ratio derived from FACS data in (b). **d.** Representative colony morphology and FT fluorescence of H2B-FT-Medium knock-in mESCs maintained in feeder-free conditions. **e.** Confirmation of cell cycle change following 48h of RA treatment, as analyzed by EdU pulse-labeling and DNA content profiling. **f.** Representative FACS plots of red vs. blue fluorescence in pluripotent and RA-treated mESCs (top). These FACS data were re-plotted as histograms of blue/red ratio (bottom). **g-h:** Pluripotent and RA-treated cells were FACS sorted according to their blue/red FT ratio. Representative gating strategy is shown. **i.** DAPI/EdU cell cycle profiles of sub-populations sorted from mESCs and RA-treated cells. **j.** Frequency of cells in G1 vs. G2/M from the FACS-sorted populations shown in (i). **k.** The number of alkaline phosphatase positive colonies formed by the same number of cells sorted in (g) following 6 days of culture. Error bars denote standard deviation across n=4 culture wells. Significance determined using student's T-Test.

Fig. 5. Virally expressed H2B-FT detects cell cycle heterogeneity of bone marrow cells. a. Representative FACS plots of blue/red profile in LKS and GMP cells from reconstituted mice 2 months

after transplantation with HSPCs virally expressing the H2B-FT reporter. **b.** Distribution of blue/red ratio in H2B-FT-expressing LKS and GMP populations, overlaid on that of whole bone marrow. **c.** FACS plots of myeloid (Mac1+) and erythroid (Ter119+) cells from reconstituted mouse bone marrow. **d.** Data from (c) plotted as histograms of blue/red H2B-FT ratio. Gates in (a) and (c) were used to exclude the H2B-FT negative cells.

Fig. 6. The proliferative landscape of live hematopoietic cells as captured by the H2B-FT reporter. **a.** Targeting strategy for the *HPRT::*TetO-H2B-FT mouse allele. **b.** DAPI/EdU cell cycle profiles of GMPs vs. early erythroid cells following 2 hours of *in vivo* EdU labeling. **c.** Distributions of H2B-FT blue/red ratio in LKS, GMPs, and early erythroid cells. **d.** Frequency of myeloid (Mac1+), B-cell (B220+), and T-cell (CD3+) lineages in peripheral blood of healthy H2B-FT knock-in mice vs. those crossed with MLL-ENL. All mice were treated with Dox for at least 8 days prior to analysis. **e.** Representative H2B-FT blue/red profiles within defined peripheral blood subsets as in (d).

Fig. 7. Estimating *in vivo* cell cycle length from H2B-FT blue/red ratio. a. Cell cycle length distribution of cultured GMPs. Individual cell cycle length was determined by time-lapse microscopy. Dotted lines show the indicated percentiles. **b.** H2B-FT blue/red ratio distribution of the same GMPs as analyzed by flow cytometry after 24 hours culture. **c.** Four paired data points of corresponding cell cycle length percentile and blue/red ratio percentile were used to derive the $C \cdot \tau_C$ value using a normalization of Equation S2b (see main text for details). Each $C \cdot \tau_C$ value (shown in bold) was then applied onto the other three blue/red ratios to generate four separate predictions of cell cycle lengths. **d.** The four predicted cell cycle length curves were compared with the actual data (solid black line). From this plot, a $C \cdot \tau_C$ value representing the average of predictions 2 and 3 was selected for estimating *in vivo* cell cycle lengths. **e.** Cell cycle length distributions of designated bone marrow populations from a representative H2B-FT mouse, calculated as illustrated in (c-d). **f.** Cell cycle length distribution of normal GMPs and L-GMPs from a representative mouse induced to express MLL-ENL. **g.** Median cell cycle length variation among three H2B-FT mice, shown by percent coefficient of variation (CV%). **h.** Cell cycle length distributions of LKS and GMP populations from the three mice. For panels (e), (f), and (h) the box plot represents the median and interquartile range of each group; whiskers represent 5th-95th percentile.

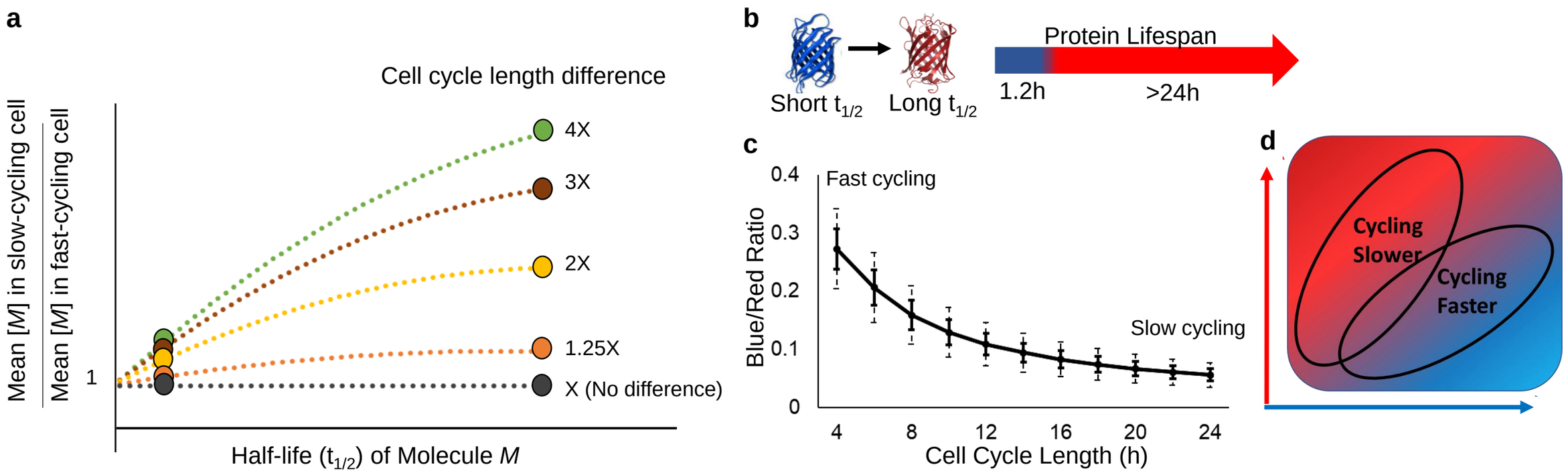

Fig. 1. Design principles of a fluorescent reporter of cell cycle speed. a. Based on Equation S1, intracellular levels of a given molecule, *M*, are predicted to depend on its molecular half-life as well as the cell cycle lengths. Here, the ratio of M's concentration in theoretical cell populations with different cycling speeds are plotted. When *M* is short-lived (circle, far left), its cellular concentration shows little difference between slow- and fast-cycling cells. However, with a long-lived *M* (circle, far right), the concentration difference increases proportionally to the difference in cell cycle lengths. **b.** The color-changing Fluorescent Timer ("FT") displays a short half-life as a blue protein, and a long half-life as a red protein. **c.** The average blue/red ratio of cells expressing the FT is predicted to drop as cell cycle lengthens (see Equation S2), providing a fluorescence-based strategy to identify cells cycling at different rates. Because the blue/red ratio fluctuates when cell cycle progresses (see Extended Data Fig. S1), the relationship between blue/red ratio and cell cycle length is best described by a probability distribution. For modeling, all cells are assumed to maintain a constant cycling rate through generations. Solid and dashed error bars denote 1 and 2 standard deviations, respectively. All FT blue/red ratio are defined as blue / (blue + red). **d.** The anticipated positions of slow and fast cycling cells on a hypothetical plot of blue and red fluorescence intensity.

Fig. 2. Characterization of the H2B-FT reporter in cultured cells. a. Schematic of inducible H2B-FT expression construct. **b.** Representative images of HeLa cells expressing the H2B-FT. **c.** Selected time series of H2B-FT fluorescence in HeLa cells from a representative field of view following doxycycline (Dox) induction. **d-e**. Quantification of average nuclear blue (**d**) and red (**e**) FT intensity over time following Dox treatment. **f.** Selected time series of HeLa cells after Dox washout at T=4.5 h. **g**. Data from (d-e) plotted as blue/red ratio. Error bars represent standard deviation across n = 3 culture wells. Nuclear intensity measurements were normalized to timepoint 0. Images were taken using a 20x objective. Scale bars: 50μm.

Fig. 3. The H2B-FT blue/red profile reflects cell proliferation rate *in vitro*. a. Changes in cell number over time in primary iH2B-FT MEFs following transduction with either c-Myc or empty vector control (EV). Error bars denote standard deviation across n=4 culture wells. **b.** The ratio of blue/red fluorescence intensity was determined for individual cells at 25h and 70h post transduction. Box plots represent the median and interquartile range and whiskers represent 5th-95th percentile. P values were calculated from Mann-Whitney test with a 99% confidence level. 25h, p= 0.295; 70h, p< 0.0001. **c.** The blue and red fluorescence level of individual cells at 70h post transduction. Each dot denotes a single cell. FACS-style gates were applied to representative scatter plots. **d.** The percentage of cells within each gate. Error bars show standard deviation across n=4 culture wells. P=0.0018 (Red Cells) and P=0.0220 (Blue Cells), determined using the Holm-Sidak test. **e.** The cell cycle lengths of individual cells from each gate were determined by image tracking. Cell cycle length represents the time interval between two consecutive mitoses within the same cell lineage. Cell cycle length is heterogeneous and the distribution of cell cycle lengths for each condition are shown as histograms. n values refer to the number of cells tracked for each condition. **f.** The relationship between cell cycle length and H2B-FT blue/red ratio. Each dot denotes an individual cell. All trackable cells (n=189) from both conditions are plotted. Spearman correlation coefficient = -0.7808. P<0.0001 was calculated with a 95% confidence interval.

Fig. 4. H2B-FT blue/red profile allows FACS sorting of live cells with different proliferative rates. a. BaF3 cells proliferate at different rates in varying IL-3 concentrations, as determined by cell counting. Error bars denote standard deviation across n=6 culture wells. **b.** Representative FACS plots of BaF3 cells expressing the H2B-FT reporter grown under different IL-3 concentrations. **c.** Histograms of blue/red fluorescence ratio derived from FACS data in (b). **d.** Representative colony morphology and FT fluorescence of H2B-FT-Medium knock-in mESCs maintained in feeder-free conditions. **e.** Confirmation of cell cycle change following 48h of RA treatment, as analyzed by EdU pulse-labeling and DNA content profiling. **f.** Representative FACS plots of red vs. blue fluorescence in pluripotent and RA-treated mESCs (top). These FACS data were re-plotted as histograms of blue/red ratio (bottom). **g-h:** Pluripotent and RA-treated cells were FACS sorted according to their blue/red FT ratio. Representative gating strategy is shown. **i.** DAPI/EdU cell cycle profiles of sub-populations sorted from mESCs and RA-treated cells. **j.** Frequency of cells in G1 vs. G2/M from the FACS-sorted populations shown in (i). **k.** The number of alkaline phosphatase positive colonies formed by the same number of cells sorted in (g) following 6 days of culture. Error bars denote standard deviation across n=4 culture wells. Significance determined using student's T-Test.

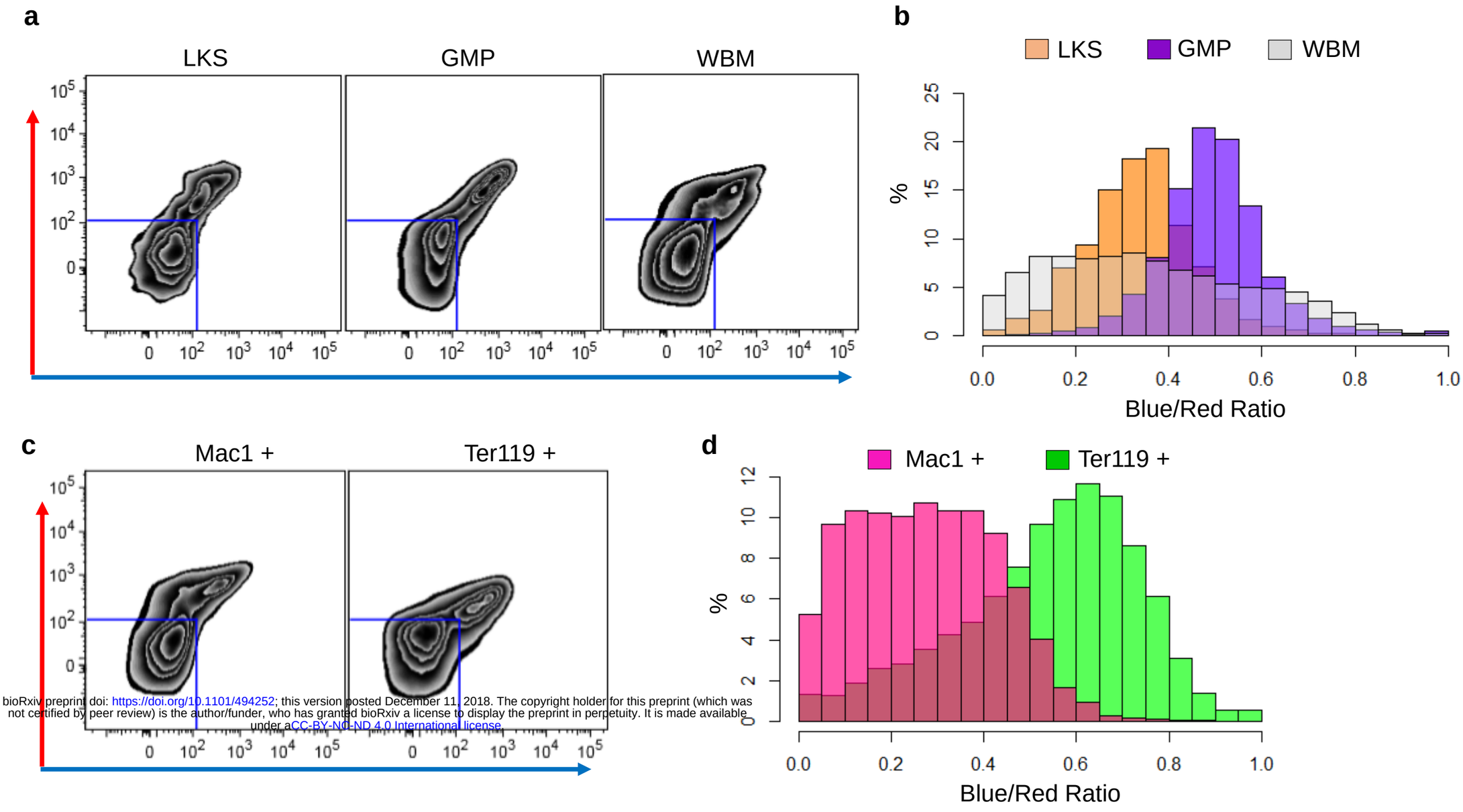

Fig. 5. Virally expressed H2B-FT detects cell cycle heterogeneity of bone marrow cells. a. Representative FACS plots of blue/red profile in LKS and GMP cells from reconstituted mice 2 months after transplantation with HSPCs virally expressing the H2B-FT reporter. **b.** Distribution of blue/red ratio in H2B-FT-expressing LKS and GMP populations, overlaid on that of whole bone marrow. **c.** FACS plots of myeloid (Mac1+) and erythroid (Ter119+) cells from reconstituted mouse bone marrow. **d.** Data from (c) plotted as histograms of blue/red H2B-FT ratio. Gates in (a) and (c) were used to exclude the H2B-FT negative cells.

Fig. 6. The proliferative landscape of live hematopoietic cells as captured by the H2B-FT reporter. a. Targeting strategy for the *HPRT::*TetO-H2B-FT mouse allele. **b.** DAPI/EdU cell cycle profiles of GMPs vs. early erythroid cells following 2 hours of *in vivo* EdU labeling. **c.** Distributions of H2B-FT blue/red ratio in LKS, GMPs, and early erythroid cells. **d.** Frequency of myeloid (Mac1+), B-cell (B220+), and T-cell (CD3+) lineages in peripheral blood of healthy H2B-FT knock-in mice vs. those crossed with MLL-ENL. All mice were treated with Dox for at least 8 days prior to analysis. **e.** Representative H2B-FT blue/red profiles within defined peripheral blood subsets as in (d).

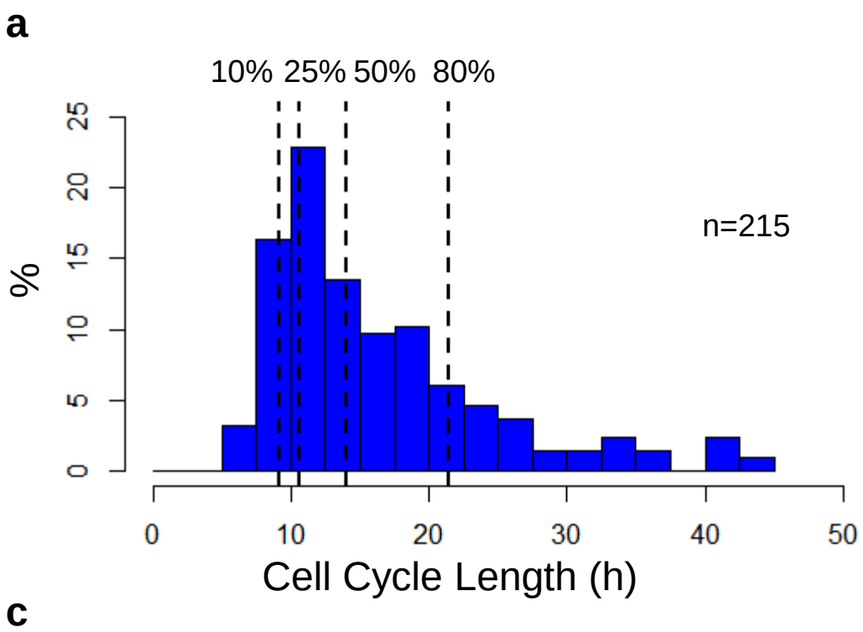

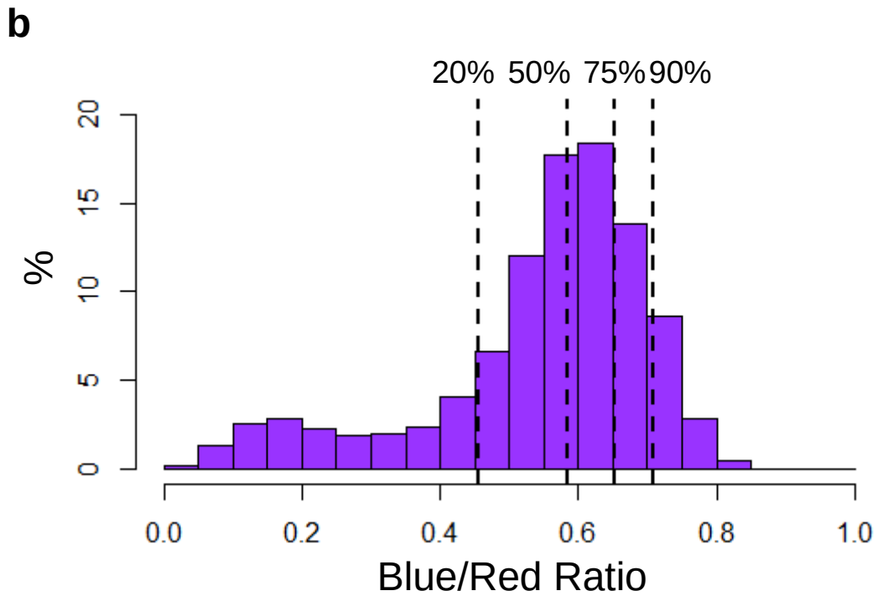

c

CC length percentile	Actual CC length (h)	Blue/red ratio percentile	Blue/red ratio value	Derived $C \cdot \tau_C$ Value	Prediction 1: CC length (h)	Prediction 2: CC length (h)	Prediction 3: CC length (h)	Prediction 4: CC length (h)
10	9.12	90	0.709	**22.22**	**9.12**	8.27	8.10	7.33
25	10.7	75	0.653	**20.14**	11.81	**10.70**	10.48	9.50
50	14	50	0.585	**19.73**	15.76	14.29	**14.00**	12.68
80	21.4	20	0.455	**17.87**	26.62	24.12	23.63	**21.40**

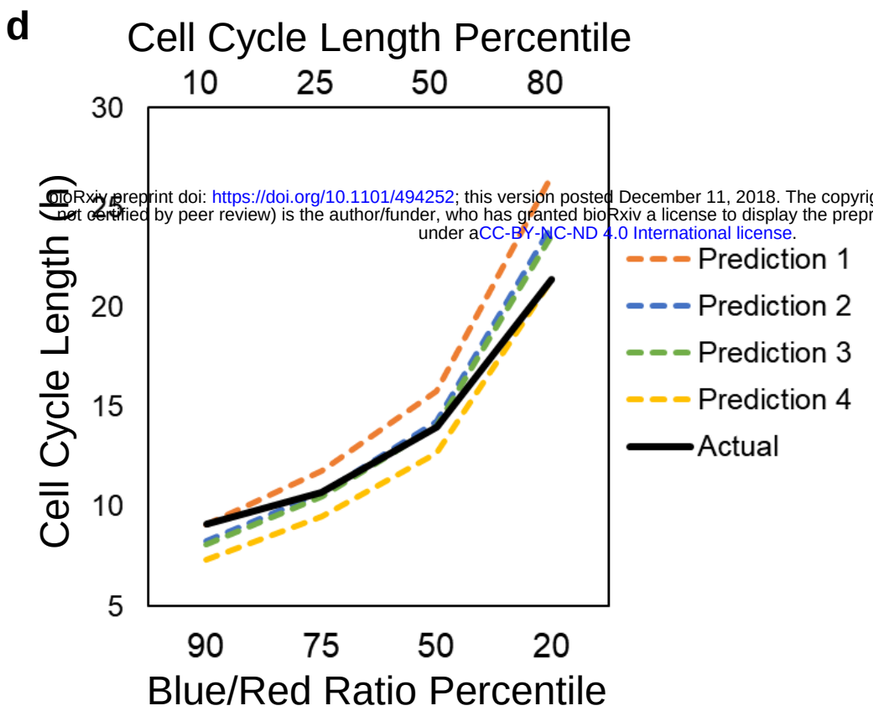

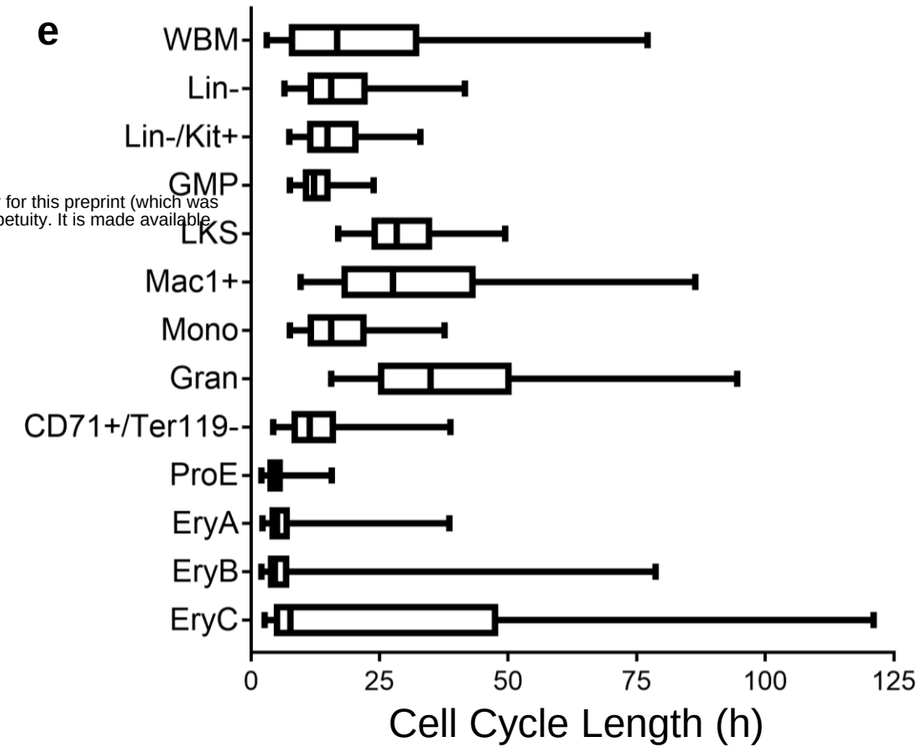

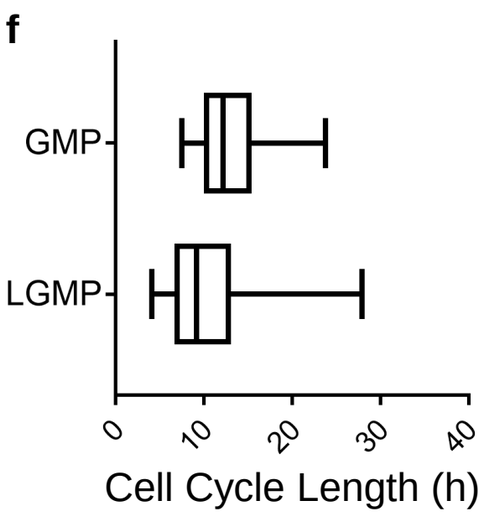

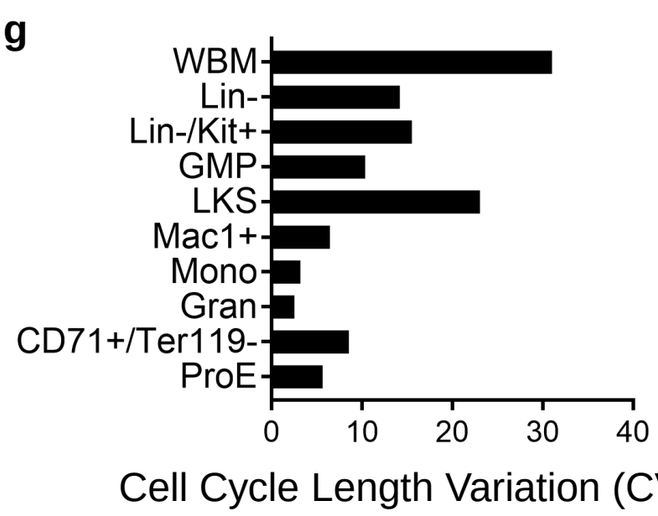

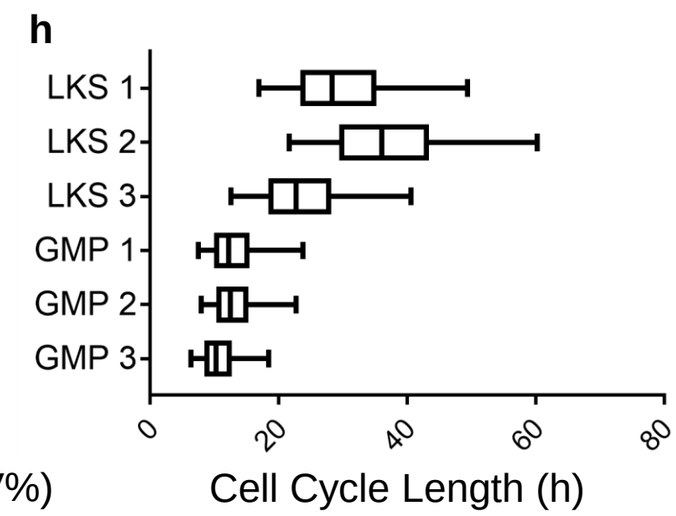

Fig. 7. Estimating *in vivo* cell cycle length from H2B-FT blue/red ratio. a. Cell cycle length distribution of cultured GMPs. Individual cell cycle length was determined by time-lapse microscopy. Dotted lines show the indicated percentiles. **b.** H2B-FT blue/red ratio distribution of the same GMPs as analyzed by flow cytometry after 24 hours culture. **c.** Four paired data points of corresponding cell cycle length percentile and blue/red ratio percentile were used to derive the $C \cdot \tau_C$ value using a normalization of Equation S2b (see main text for details). Each $C \cdot \tau_C$ value (shown in bold) was then applied onto the other three blue/red ratios to generate four separate predictions of cell cycle lengths. **d.** The four predicted cell cycle length curves were compared with the actual data (solid black line). From this plot, a $C \cdot \tau_C$ value representing the average of predictions 2 and 3 was selected for estimating *in vivo* cell cycle lengths. **e.** Cell cycle length distributions of designated bone marrow populations from a representative H2B-FT mouse, calculated as illustrated in (c-d). **f.** Cell cycle length distribution of normal GMPs and L-GMPs from a representative mouse induced to express MLL-ENL. **g.** Median cell cycle length variation among three H2B-FT mice, shown by percent coefficient of variation (CV%). **h.** Cell cycle length distributions of LKS and GMP populations from the three mice. For panels (e), (f), and (h) the box plot represents the median and interquartile range of each group; whiskers represent 5th-95th percentile.